Comparative analysis of rolling contact fatigue life in a wind turbine pitch bearing with different modeling approaches

Journal of Physics: Conference Series **2767** (2024) 052036 doi:10.1088/1742-6596/2767/5/052036

Comparative analysis of rolling contact fatigue life in a wind turbine pitch bearing with different modeling approaches

Ashkan Rezaei[1], Florian Schleich[2], Oliver Menck[2], Matthis Grassmann[2], Arne Bartschat[2] and Amir R. Nejad[1]

[1] Department of Marine Technology, Norwegian University of Science and Technology (NTNU), NO-7491, Trondheim, Norway
[2] Fraunhofer Institute for Wind Energy Systems (IWES), Large Bearing Laboratory, Am Schleusengraben 22, 21029 Hamburg, Germany

E-mail: ashkan.rezaei@ntnu.no

Abstract. The load calculation for wind turbines usually does not take pitch bearings into account, and the pitch-bearing internal load distribution is calculated in a decoupled process. In the current study, a coupled wind turbine load simulation considering the pitch bearings is proposed. Internal pitch-bearing load distribution and roller contact fatigue life are compared to a decoupled approach using a high-fidelity finite-element model. Internal pitch-bearing load distribution can be an essential variable in almost all major pitch-bearing failures. Furthermore, rolling contact fatigue is one of the major types of pitch-bearing failure that can represent the bearing service life. The results show that the flexibility of the surroundings has an effect on the contact forces. As a result, the finite element model-based life calculation of the NREL 5 MW turbine predicts a longer rolling contact fatigue life for the bearing than the multi-body system-based one. For the IWT7.5, sample load cases indicate that this behavior is different, leading to the conclusion that the life of the bearing is significantly affected by the stiffness of the bearing and its surrounding components.

1. Introduction

There are two general types of failure in the pitch bearing: subsurface failure, which consists of rolling contact fatigue, core crushing, edge loading, and ring fracture; and surface-initiated failure, which consists of rotational wear, fretting, and false brinelling [1]. In terms of failure criteria, damage causes, application environments, and overall bearing requirements, different bearing applications show significant variations [2]. Pitch bearings are subject to two main failure modes [1, 3]. The first one is the ring fracture. The second one is the rolling contact fatigue of the bearing, where all the possible damage starts at the contact point between the rolling elements and raceways. If the load of the bearing is calculated correctly and the bearing is mounted, lubricated, and maintained appropriately, one can expect that the service life of the bearing will be determined by raceway fatigue [4].

Little research has been done on pitch-bearing modeling in large wind turbines to determine the load distribution among the rolling bodies. In 2009, the National Renewable Energy Laboratory (NREL) published a pitch and yaw bearing design guideline 03 (DG03) [5]. However,

it is under study to revise [6]. It has been commonly used in the wind industry as a guideline for determining the rating life of the pitch bearing [7]. DG03 uses two approaches. Firstly, it uses an equation that is based on the external loads (forces and moments) and the pitch circle diameter of the bearing. This approach does not consider the internal details of the bearing. The second approach presented by DG03 is similar to the ISO/TS 16281 [8] approach. The ISO/TS 16281 approach, which is based on the individual rolling element loads, calculates the individual lifetime of each raceway.

Menck et al. [9] studied ISO/TS 16281 together with NREL's approaches. They used aeroelastic loads to perform a large number of finite element (FE) simulations and determined the resulting internal bearing loads using a regression for any desired operating condition of the turbine. They observed that the simplified method used by NREL exhibits qualitative behavior that is very similar to the other two methods. They proposed an adjustment to the moment's coefficient from 2 to 2.5. Leupold et al. [10] simulated a 3 MW wind turbine and pitch bearing in *Simpack* software, and the damage to the raceways was calculated. They compared the result of multi-body simulation (MBS) with a FE model (FEM) of a blade with a hub and a point load on the blade. Recently, Graßmann et al. [11] evaluated the FEM result of the blade-bearing raceway with extensive experiments on the pitch bearing.

In this paper, the study intends to compare the different modeling approaches and their influences on the internal load distribution and calculated fatigue life. This paper is structured into four sections. In the next section, the methodology is described, which consists of the reference wind turbines (RWTs) together with the different modeling approaches and the nominated load cases. Additionally, the pitch bearings' specifications are presented. The results are described afterward, and the discussion presents the findings with respect to load distributions and life. In the end, the conclusion is stated.

2. Methodology

2.1. Reference wind turbines

The nominated wind turbines are the NREL 5 MW wind turbine [12] and the IWES Wind Turbine IWT-7.5, designed by Fraunhofer IWES and described by Popko et al. [13]. The wind turbine configurations are given in Table 1.

Table 1: Nominated reference wind turbine specifications [12], [13]

Wind Turbine	NREL 5 MW	IWT 7.5MW
Rating (MW)	5	7.54
Rotor Diameter (m)	126	163.4
Hub Height (m)	90	120
Minimum, Rated Rotor Speed (rpm)	6.9, 12.1	5, 10
Cut-In, Rated, Cut-Out Wind Speed (m/s)	3, 11.4, 25	3, 11.7, 25
Shaft Tilt, Precone (°)	5, 2.5	5, 2
Rotor Mass (t)	110	196.78
Nacelle Mass (t)	240	340
Tower Mass (t)	347.46	1467.355

The related pitch-bearing specifications for 5 MW and 7.5 MW reference wind turbines are presented in [14] and [15], respectively. The pitch-bearing configurations are given in Table 2.

Table 2: Pitch-bearing specifications of nominated reference wind turbines [12], [13]

Pitch bearing	NREL 5 MW	IWT 7.5MW
Ball diameter (mm)	75	80
Contact angle (°)	45	45
Pitch circle diameter (mm)	3558	4690
Number of balls	125	147
Inner raceway radius (mm)	39.75	42.55
Outer raceway radius (mm)	39.75	42.55
Number of row	2	2

2.2. Wind turbine and pitch-bearing simulation approaches

The wind turbine and pitch bearing are simulated in two different ways. On the one hand, the simulation is performed in *OpenFAST* software [16], and the result is mapped to the FEM. The contact forces are derived from FEM results. The FEM models of the considered RWTs are shown in Fig. 1.

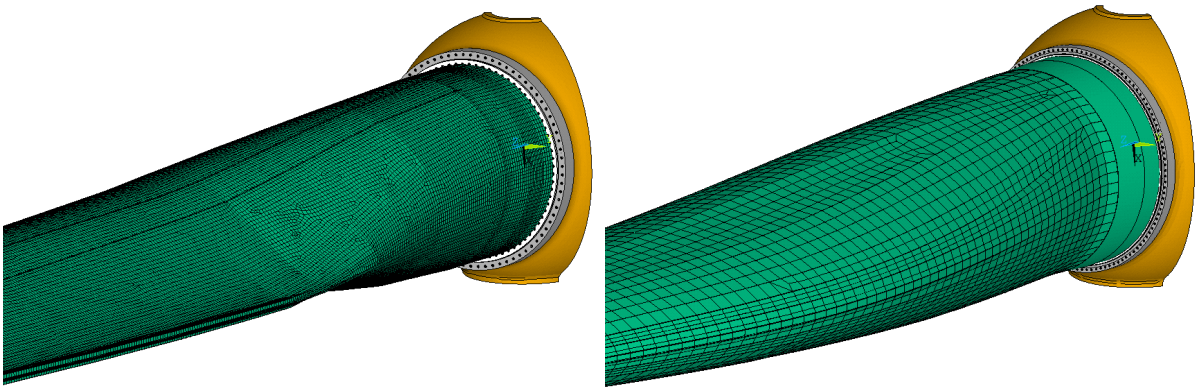

Figure 1: Finite element model of the NREL 5 MW wind turbine rotor (left) and the IWT 7.5 MW wind turbine rotor (right)

The IWT7.5 MW FE model is the same as used by Menck et al. [9], and the FE model of the NREL 5 MW turbine builds up in the same way to have an appropriate basis for a comparison. As shown in Fig. 1, both turbine FE models consider one-third of the full rotor to save computational time. At the hub's cutting planes, cyclic constraints make the models behave symmetrically. In turn, certain load situations caused by three individually loaded blades cannot be considered properly, which is assumed to be negligible for the following comparative study. However, it should be noted that this simplification should be avoided in a detailed load calculation of the blade bearings. The hub model of the NREL 5 MW turbine is a down-scaled version of the IWT7.5 hub model. In both models, shell elements are used to model the blade, which connects to a stiffener plate that is mounted to the bearing's inner ring. Always-bonded contacts are defined to connect all components with each other.

Both bearings are double-row four-point contact ball bearings with a total of 250 (NREL 5 MW) and 294 (IWT 7.5 MW) balls. Each ball is in contact with the raceway at four points, which leads to a large number of frictional contacts in the bearings. To save computational effort, the FE bearing models represent the ball-raceway interactions with nonlinear spring elements. The springs connect the curvature centers of two opposite raceways. Two springs represent one ball. Force-distributed constraints (FDCs) connect the spring elements with the

raceways. The bearing rings are divided into equidistant segments according to the number of balls. For each segment, the surface of the raceway is linked to the springs. Fig. 2 shows the modeling approach with the spring elements in orange, the linked part of the raceway in green, and the FDCs indicated in blue. Further details of the verification and validation of this modeling approach can be found in [11].

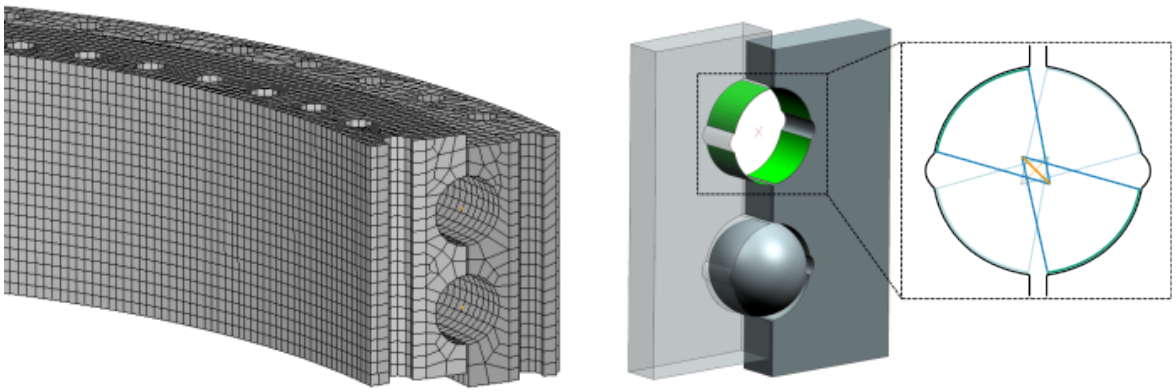

Figure 2: Modeling approach of double-row four-point contact ball bearings using nonlinear spring elements [11]

For the IWT7.5 rotor FE model, load distributions at 358 simulation points were used to generate an interpolation grid for the bearing lifetime calculation. With the NREL 5MW rotor FE model, only 140 simulations are carried out as the maximum occurring pitch angle is significantly smaller compared to the one of the IWT7.5, and in turn, with the same pitch angle increment of 10°, the resulting simulation grid contains significantly fewer simulation points.

On the other hand, the models in the *Simpack* software were developed to simulate the wind turbine and pitch bearing simultaneously. *Simpack* is a general multi-body system simulation software that enables analysts and engineers to simulate the non-linear motion of mechanical or mechatronic systems [17]. The pitch bearing was modeled with force element 88 in the software. This force element allows one to model the forces and torques transmitted by ball or roller bearings. This force element calculates detailed forces and torques transmitted by rolling bearings, considering geometrical bearing properties compatible with ISO 16281 [8]. The calculation considers nonlinear stiffness characteristics and cross-coupling effects. The contact forces in every rolling element of the pitch bearing are extracted directly from the force element output of the software. In Fig. 3, the MBS models are depicted.

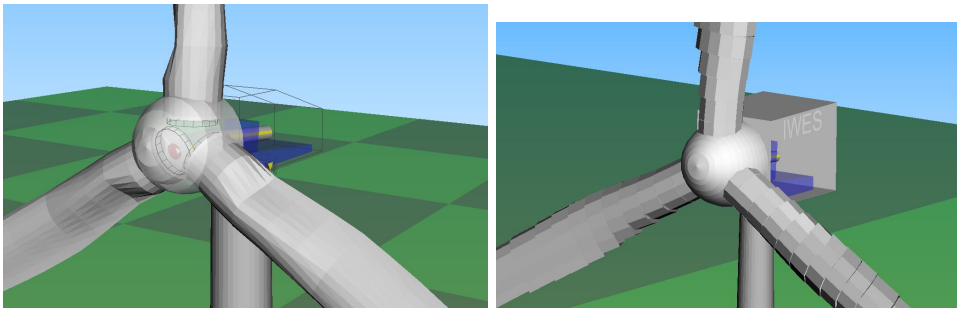

Figure 3: Multi-body system model of the NREL 5 MW wind turbine (left) and the IWT 7.5 MW wind turbine (right)

Aeroelastic simulations are carried out according to IEC 61400-1 [18], DLC 1.2. According to DLC 1.2, the wind regime is a normal turbulence model (NTM), and it consists of different average wind speeds from cut-in to cut-out with an interval of 2 m/s in six different wind seeds. Yaw errors of +8 and -8 along with 0 are considered in each average wind speed and seed. It results in 216 simulations for every model. Each simulation takes 700 seconds; the results of the first hundred seconds are not considered.

2.3. Rolling contact fatigue life

The rolling contact fatigue life is calculated according to the Finite Segment Method [19]. To this end, each raceway is separated into M segments of finite width. The ball movement relative to each raceway is evaluated for each timestep of the aeroelastic simulation, and relative movement from one segment to another is counted as a load cycle for the segment that the ball left. The load is then determined, either by using the Simpack or the FE load distribution, for each individual segment that experiences a load cycle in a given step. Using this approach, it is possible to determine the varying fatigue loading around the circumference of the bearing. The effect of controller movement and differences in load distribution on fatigue loading around the bearing can be shown.

The Finite Segment Method is based on ISO 281 [20] and thus also closely related to life calculation approaches such as that in NREL DG03 [5] and ISO/TS 16281 [8]. As argued in [19], the Finite Segment Method captures local effects of the load cycle history more accurately than approaches such as that found in NREL DG03. This means that small oscillations in varying positions can be accurately captured without losing information prior to calculating the final bearing life, and the influence of varying load distributions and directions of the load over time can be accurately captured, too. As opposed to ISO/TS 16281, which calculates the life based on the load distribution for one load case, the life is calculated only after all load cycles with the respective load distribution at their respective times have been taken into account.

The figures in this document show the value $\ln(1/S_m)$, which can be considered a measure of the fatigue-relevant damage for each segment m. It contains the survival probability S_m of each segment m.

3. Results and discussion

Internal bearing load distributions of the bearing on each raceway in different models and approaches were calculated. The results of the load distribution for two load cases, $M_{\mathrm{res}} = 6.6\,\mathrm{MNm}$ and $16.5\,\mathrm{MNm}$, for NREL 5 MW as well as those for $M_{\mathrm{res}} = 10\,\mathrm{MNm}$ and $25\,\mathrm{MNm}$ on the IWT7.5 are depicted in Fig. 4. The raceway positions are shown in Fig. 5. Both load cases use a load angle of 90° and a pitch angle of 0°. Both of these angles affect the FEM results due to the non-rotationally symmetrical stiffness of the bearing's surrounding components as well as the flexibility of the bearing, but they do not affect the MBS results.

For the NREL 5 MW simulations, comparing the MBS to the FEM results, the maximum rolling element load Q in the bearing is higher in the MBS simulations. This is due to the FEM model considering contact angle changes, which the MBS model cannot accurately capture since it uses stiff surrounding structures, with the only flexibility in the MBS model stemming from the Hertzian rolling bodies. In the FEM model, the bearing ring is modeled accurately as flexible and therefore deforms to accommodate the higher loads. This results in higher contact angles α. Fig. 6 shows a ball reacting to an external axial force F_{a}. Irrespective of α, the axial component Q_{a} contributing to the total load Q must equal F_{a}; but for lower contact angles, the radial component Q_{r} must be higher, resulting in a higher rolling element load Q for the MBS model.

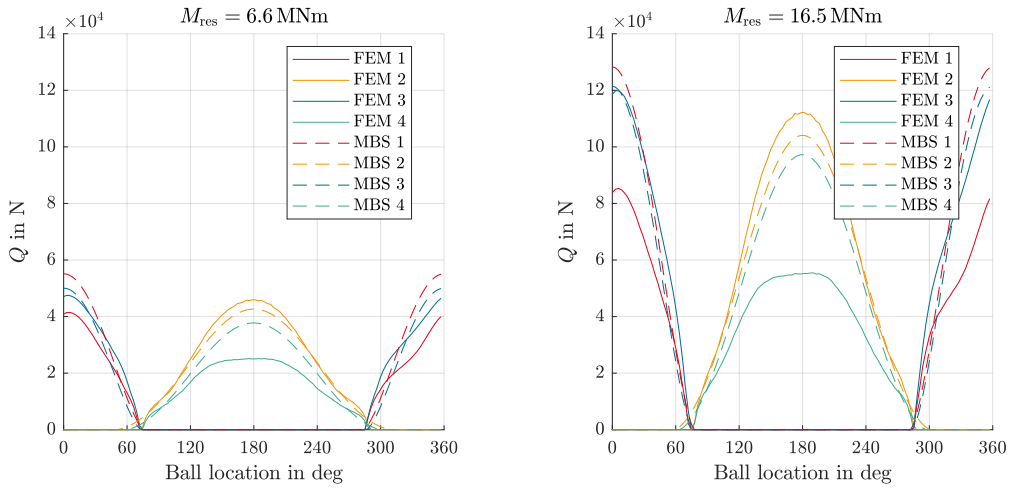

(a) NREL 5 MW, $M_{res} = 6.6$ MNm and 16.5 MNm for FEM and MBS

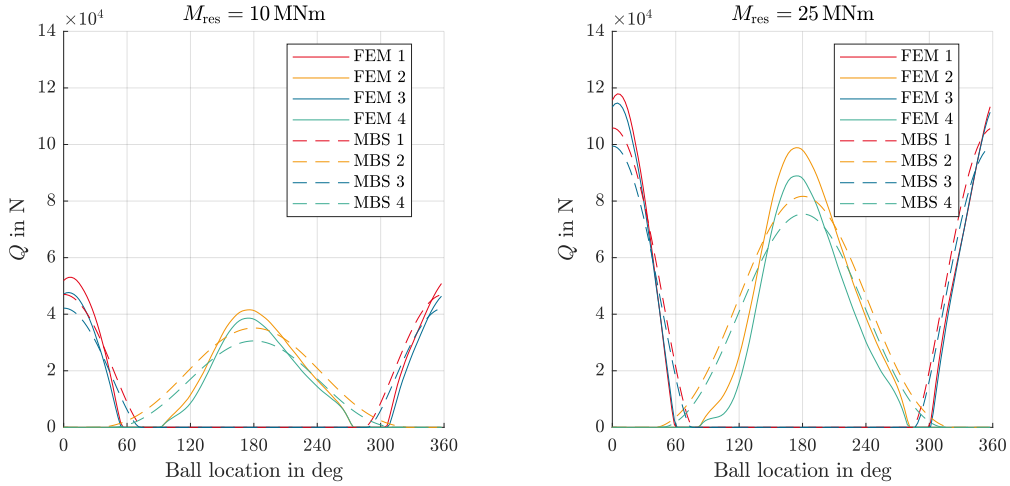

(b) IWT 7.5 MW, $M_{res} = 10$ MNm and 25 MNm for FEM and MBS

Figure 4: Bearing load distribution with FEM and MBS for different bending moments and with a pitch angle of 0° and a load angle of 90°, for raceways 1 to 4 each

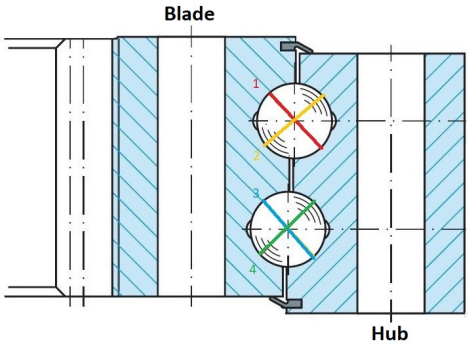

Figure 5: Raceways position in the pitch bearing

Aside from these differences in maximum rolling element load, it can be seen that the load distributions on raceways 1 and 3, as well as 2 and 4, are more similar in the MBS model than in the FEM model. This, too, is a result of the flexible rings in the FEM model, which deform and thus result in stronger discrepancies between the raceway loads than the MBS model does, in which there is no ring deformation. The FEM model even predicts the highest load to occur at raceway 1 for both simulated load cases, while the MBS model predicts it to occur at raceway 3, again demonstrating the necessity of flexible rings for an accurate determination of rolling element loads within the bearing.

These details differ for the IWT7.5 simulations. For the IWT7.5, the highest rolling element load occurs in the FEM simulations, while the MBS ones are consistently lower for all raceways. This is due to the stiffness of the rotor blade not being rotationally symmetrical. The spar caps in the rotor blade lead to a local increase in stiffness, which increases the maximum rolling element load Q at the 0° and 180° positions in the bearing. This effect has also been seen in [21], where a roller bearing was simulated, in which the contact angle changes described above for the NREL 5 MW simulations do not occur. While the given IWT7.5 simulations also experience contact angle increases, which, as detailed above, should reduce the maximum load Q, the increased local stiffness caused by the spar caps competes with this effect and appears to overrule it for the given IWT7.5 simulations.

Aside from these big differences to the NREL 5 MW simulations, there are some smaller ones: For the IWT7.5 FEM simulations, raceways 1 and 3 are very similar to each other, as are raceways 2 and 4. Moreover, unlike the FEM-modeled NREL 5 MW load cases shown here, the referenced IWT7.5 results show the highest rolling element loads to appear on raceway 1. The specifics of the FEM load distributions are thus dependent on the design of the bearing and its surrounding structures and can differ a lot between different turbines.

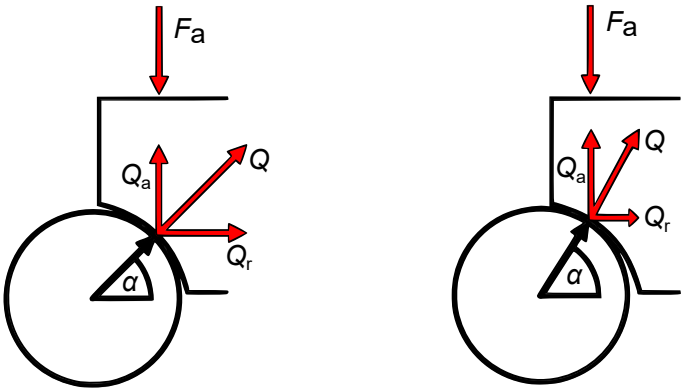

Figure 6: The effect of different contact angles on rolling element load Q for identical loads F_a acting on the bearing. Left: Contact angle as in MBS; right: increased contact angle as in FEM results in lower load Q for NREL 5 MW

The internal load distributions of the NREL 5 MW turbine were used to calculate the rolling contact fatigue life of the blade bearings. The results of the rolling contact fatigue life are presented in Table 3. The calculated life of the FEM-based calculations is higher than that of the MBS-based calculations using Simpack. This is due to the difference in rolling body loads on the NREL 5 MW turbine discussed above: the FEM model more accurately captures the contact angle changes that occur in the bearing and therefore obtains lower contact forces, which in turn result in a higher rolling contact fatigue life of the bearing.

Table 3: Rolling contact fatigue life of pitch bearing in the NREL 5 MW turbine for FEM and MBS

Pitch bearing	NREL 5 MW, FEM	NREL 5 MW, MBS
L_{10} in years	11.35	7.25

Fig. 7, depicts the value $\ln(1/S_m)$ after 20 years of operation of the 5 MW NREL wind turbine as a measure of damage. The points in the diagram represent segments of the inner and outer raceways. The results show the same trend as the load distributions given in Fig. 4: For the FEM model, loads on raceways 3 and 2 appear to be the highest, resulting in the highest rolling contact fatigue damage. The loads on raceway 4 are the lowest, and due to the exponential relationship between load and life, they cause very little damage with respect to rolling contact fatigue. For the MBS model, on the other hand, loads on raceway 1 are highest and correspondingly cause the highest damage, more than on raceway 3, the reverse of the behavior in the FEM model.

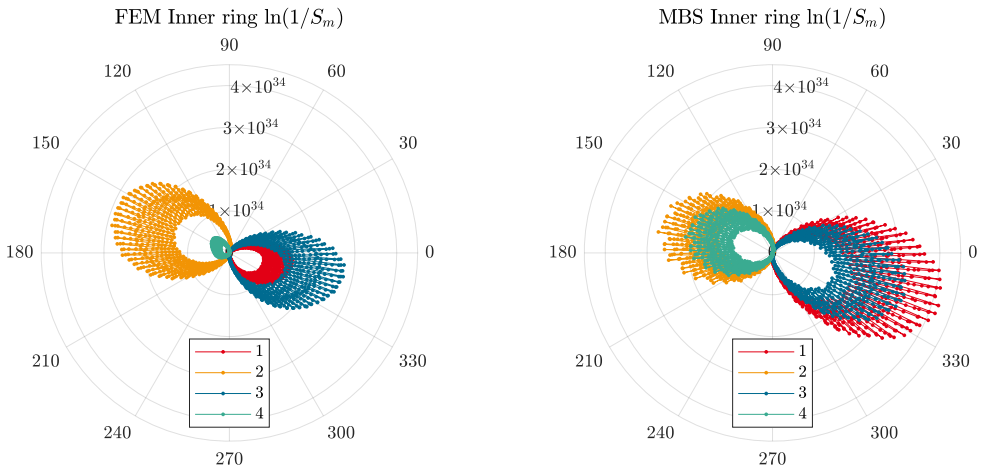

(a) NREL 5 MW, FEM and MBS

Figure 7: Damage index $\ln(1/S_m)$ for the inner ring after 20 years of operation, FEM and MBS, for raceways 1 to 4 each

4. Conclusion

The rolling contact fatigue life of a blade bearing on the NREL 5 MW turbine was calculated using loads determined from FEM via post-processing after the aeroelastic simulations, as well as using a Simpack-based MBS model directly embedded into the aeroelastic simulations. The FEM model showed lower overall contact forces due to the flexibility of the model, which allowed for higher changes in the contact angle. For the studied cases in this paper, these changes reduce radial components on the rolling elements and therefore reduce rolling element loads caused by otherwise identical external loads compared to the MBS model. By increasing the model complexity of the neighboring components, the load distribution of the bearing in MBS will be more accurate.

Consequently, the calculated rolling contact fatigue life of the bearing is higher in the FEM-based life calculation than in the MBS-based one. The overall lower FEM loads cause less fatigue damage to the raceways than the MBS ones. Discrepancies between raceway damage are also much higher in the FEM-based life calculation than in the MBS-based one, again due to the

higher and more accurate structural deformation in the FEM model as compared to the MBS one.

For two sample load cases of the IWT7.5, these trends appeared to be different. The local stiffness increase caused by the spar caps in the rotor blade increased the rolling element loads in the FEM simulations compared to the MBS ones. This effect overruled the lowering of rolling element loads, which results from contact angle increases in the FEM model. The specifics of the blade bearing load distribution therefore depend on the particular blade bearing design and that of its surrounding structures, which can change between different turbines.

Acknowledgments
The first author gratefully acknowledges the financial support from Equinor for a short stay at Fraunhofer IWES. Fraunhofer IWES gracefully acknowledges funding from the German Federal Ministry for Economic Affairs and Climate Action (BMWK) (Grant reference number 03EE3065).

References

[1] Andreasen D K, Rodenas-Soler C, Oertel U, Krugel K, Reinares I, Mendia I S, Nielsen J H, Olsen A, Tinni A, Vizireanu D, Cheaytani J, Kratz M and Bousseau P 2022 Portability of failure mode detection/prognosis orientations 2.0 Tech. rep. ROMEO URL `https://www.romeoproject.eu/wp-content/uploads/2022/10/D2_4_Portability_2_3_final.pdf`

[2] de la Presilla R, Wandel S, Stammler M, Grebe M, Poll G and Glavatskih S 2023 *Tribology International* **188** 108805 ISSN 0301-679X URL `https://www.sciencedirect.com/science/article/pii/S0301679X23005935`

[3] Reinares I, Bousseau P, Cheaytani J, Krugel K, Oertel U, González E, Sainz I, Ortiz R and Rodenas C 2019 Failure mode diagnosis/prognosis orientations 2.1 Tech. rep. ROMEO URL `https://www.romeoproject.eu/wp-content/uploads/2019/06/D2.1_ROMEO_Failure_mode_diagnosis_prognosis_orientations.pdf`

[4] Stammler M, Thomas P, Reuter A, Schwack F and Poll G 2020 *Wind Energy* **23** 274–290

[5] Harris T, Rumbarger J and CP B 2009 Wind turbine design guideline dg03: Yaw and pitch rolling bearing life Tech. rep. NREL/TP-500-42362, National Renewable Energy Lab.(NREL), Golden, CO (United States)

[6] Stammler M, Menck O, Guo Y and Keller J 2023 The wind turbine design guideline DG03: Yaw and pitch rolling bearing life revisited – an outline of suggested changes: Preprint Tech. rep. NREL/CP-5000-84797, National Renewable Energy Lab.(NREL), Golden, CO (United States) URL `https://doi.org/10.2172/969722`

[7] DNV 2016 DNV-ST-0361, machinery for wind turbines

[8] ISO 2008 Iso/ts 16281:2008, rolling bearings – methods for calculating the modified reference rating life for universally loaded bearings

[9] Menck O, Stammler M and Schleich F 2020 *Wind Energy Science* **5** 1743–1754

[10] Leupold S, Schelenz R and Jacobs G 2021 *Forsch. Ingenieurwes* **85** 211–218

[11] Graßmann M, Schleich F and Stammler M 2023 *Finite Elements in Analysis and Design* **221** 103957 ISSN 0168-874X URL `https://www.sciencedirect.com/science/article/pii/S0168874X23000501`

[12] Jonkman J, Butterfield S, Musial W and Scott G 2009 Definition of a 5-MW reference wind turbine for offshore system development Tech. rep. National Renewable Energy Lab.(NREL), Golden, CO (United States)

[13] Popko W, Thomas P, Sevinc A, Rosemeier M, Bätge M, Braun R, Meng F, Horte D, Balzani C, Bleich O *et al.* 2018 Iwes wind turbine iwt-7.5-164 rev 4 Tech. rep. Fraunhofer Institute for Wind Energy Systems IWES, Bremerhaven

[14] Rezaei A, Guo Y, Keller J and Nejad A R 2023 *Forschung im Ingenieurwesen* **87** 321–338

[15] Stammler M 2020 *Endurance test strategies for pitch bearings of wind turbines* (Stuttgart: Fraunhofer Verlag)

[16] NREL Openfast `https://github.com/OpenFAST/openfast` [Online; accessed 2 July 2022]

[17] Dassault Systèmes Simulia Corp Simpack 2023.1 documentation

[18] IEC 61400-1: 2019 wind energy generation system, part 1: Design requirements URL `https://webstore.iec.ch/publication/26423`

[19] Menck O 2023 *Journal of Tribology* **145** ISSN 0742-4787

[20] ISO 2010 Iso 281:2007, rolling bearings – dynamic load ratings and rating life

[21] Stammler M, Baust S, Reuter A and Poll G 2018 *Journal of Physics: Conference Series* **1037** 042016 ISSN 1742-6588